Imaging, Diagnosis, Prognosis

Clinical Cancer Research

Absolute Quantification of [^{11}C]docetaxel Kinetics in Lung Cancer Patients Using Positron Emission Tomography

Astrid A.M. van der Veldt[1], Mark Lubberink[1], Henri N. Greuter[1], Emile F.I. Comans[1], Gerarda J.M. Herder[4], Maqsood Yaqub[1], Robert C. Schuit[1], Arthur van Lingen[1], S. Nafees Rizvi[1], Martien P.J. Mooijer[1], Anneloes Y. Rijnders[1], Albert D. Windhorst[1], Egbert F. Smit[2], N. Harry Hendrikse[1,3], and Adriaan A. Lammertsma[1]

Abstract

Purpose: Tumor resistance to docetaxel may be associated with reduced drug concentrations in tumor tissue. Positron emission tomography (PET) allows for quantification of radiolabeled docetaxel ([^{11}C]docetaxel) kinetics and might be useful for predicting response to therapy. The primary objective was to evaluate the feasibility of quantitative [^{11}C]docetaxel PET scans in lung cancer patients. The secondary objective was to investigate whether [^{11}C]docetaxel kinetics were associated with tumor perfusion, tumor size, and dexamethasone administration.

Experimental Design: Thirty-four lung cancer patients underwent dynamic PET–computed tomography (CT) scans using [^{11}C]docetaxel. Blood flow was measured using oxygen-15 labeled water. The first 24 patients were premedicated with dexamethasone. For quantification of [^{11}C]docetaxel kinetics, the optimal tracer kinetic model was developed and a noninvasive procedure was validated.

Results: Reproducible quantification of [^{11}C]docetaxel kinetics in tumors was possible using a noninvasive approach (image derived input function). Thirty-two lesions (size $\geq$4 cm^3) were identified, having a variable net influx rate of [^{11}C]docetaxel (range, 0.0023–0.0229 mL·cm^{-3}·min^{-1}). [^{11}C]docetaxel uptake was highly related to tumor perfusion (Spearman's $\rho = 0.815$; $P < 0.001$), but not to tumor size (Spearman's $\rho = -0.140$; $P = 0.446$). Patients pretreated with dexamethasone showed lower [^{11}C]docetaxel uptake in tumors ($P = 0.013$). Finally, in a subgroup of patients who subsequently received docetaxel therapy, relative high [^{11}C]docetaxel uptake was related with improved tumor response.

Conclusions: Quantification of [^{11}C]docetaxel kinetics in lung cancer was feasible in a clinical setting. Variable [^{11}C]docetaxel kinetics in tumors may reflect differential sensitivity to docetaxel therapy. Our findings warrant further studies investigating the predictive value of [^{11}C]docetaxel uptake and the effects of comedication on [^{11}C]docetaxel kinetics in tumors. *Clin Cancer Res; 17(14); 4814–24. ©2011 AACR.*

Introduction

Docetaxel belongs to the family of taxanes, a class of drugs that binds to microtubules and subsequently induces cell cycle arrest and apoptosis (1). Docetaxel is widely used for systemic therapy of several solid malignancies, including lung cancer (2). However, clinical failure of docetaxel therapy remains a major problem, and often patients are subjected to therapy-related toxicity without gaining benefit. As response to anticancer drugs is, at least in part, thought to depend on achieving sufficient drug levels in tumor tissue, assessment of docetaxel uptake in tumors *in vivo* may be useful to understand treatment failure in patients.

To this end, docetaxel was labeled with the short-lived positron emitting radionuclide carbon-11, resulting in [^{11}C]docetaxel with an identical molecular structure as the drug docetaxel itself (3, 4). Using [^{11}C]docetaxel and positron emission tomography (PET), microdosing studies can be carried out to monitor pharmacokinetics and pharmacodynamics of docetaxel noninvasively in patients. In a previous safety study, [^{11}C]docetaxel showed high accumulation in liver (5, 6), whereas concentrations in the chest were low (6). These biodistribution data indicate that [^{11}C]docetaxel may be a suitable PET tracer for measuring docetaxel kinetics in thoracic tumors.

Authors' Affiliations: [1]Department of Nuclear Medicine & PET Research, [2]Department of Pulmonology, [3]Department of Clinical Pharmacology & Pharmacy, VU University Medical Center, Amsterdam, The Netherlands; and [4]Department of Pulmonology, St Antonius Hospital, Nieuwegein, The Netherlands

Note: Supplementary data for this article are available at Clinical Cancer Research Online (http://clincancerres.aacrjournals.org/).

This study was partly presented at the 2010 ASCO Annual Meeting, Chicago, Illinois, June 4–8, 2010, #2543; at the SNM Annual Meeting, Salt Lake City, Utah, June 5–9, 2010, #449; and at the 22nd EORTC-NCI-AACR symposium, Berlin, November 16–19, 2010, #576.

Corresponding Author: A.A.M. van der Veldt, VU University Medical Center, Department of Nuclear Medicine & PET Research, P.O. Box 7057, 1007 MB Amsterdam, The Netherlands. Phone: + 31 20 444 4214; Fax: + 31 20 444 3090; E-mail: aam.vanderveldt@vumc.nl

doi: 10.1158/1078-0432.CCR-10-2933

©2011 American Association for Cancer Research.

Downloaded from http://aacrjournals.org/clincancerres/article-pdf/17/14/4814/1997884/4814.pdf by guest on 09 October 2024

Translational Relevance

Docetaxel is an effective drug for the treatment of patients with several advanced malignancies including breast cancer, prostate cancer, and lung cancer. However, a number of patients will not benefit from docetaxel therapy. Tumor resistance to docetaxel may be associated with reduced drug concentrations in tumor tissue. Positron emission tomography (PET) is a noninvasive technique that can be used to quantify kinetics of radiolabeled docetaxel ([^{11}C]docetaxel) in tumors. The present study shows the feasibility and potential clinical relevance of quantitative [^{11}C]docetaxel PET studies in patients with lung cancer. In the future, microdosing studies using [^{11}C]docetaxel may be used to predict benefit from docetaxel in individual patients. In addition, PET imaging with [^{11}C]docetaxel may be useful for evaluating effects of other drugs on docetaxel delivery to tumors and to optimize drug scheduling.

To assess whether a microdose [^{11}C]docetaxel scan can be used to predict response to docetaxel therapy, quantification of [^{11}C]docetaxel uptake in tumor tissue is needed. This, in turn, requires the development of a tracer kinetic model, describing tumor [^{11}C]docetaxel kinetics in relation to the time course in arterial plasma (delivery). Arterial blood sampling, however, is less suited for routine clinical studies. Dynamic PET scans of the chest provide the possibility to noninvasively generate an image derived input function (IDIF) based on the time course in, for example, the ascending aorta. As the accuracy of an ascending aorta IDIF depends on the biodistribution of a tracer, this procedure needs to be validated also for [^{11}C]docetaxel.

Uptake of docetaxel in a tumor depends, at least in part, on its delivery through the circulation, which may be regulated by both drug exposure and tumor perfusion. Docetaxel exposure is reflected by clearance of [^{11}C]docetaxel from blood. Tumor perfusion can be measured using oxygen-15 labeled water ([^{15}O]H_2O), which is a freely diffusible PET tracer (7). Tumor size may also affect docetaxel delivery, as central necrotic areas with reduced tumor perfusion may develop with increasing tumor size (8).

In addition, efflux pumps may affect the concentration of radiolabeled drugs in tumors. Docetaxel is a substrate for the efflux transporter ABCB1 (formerly known as P-glycoprotein or MDR1; ref. 9). In this respect, the glucocorticoid dexamethasone, which is given as standard premedication to prevent several docetaxel-induced toxicities (10, 11), is of particular interest, because dexamethasone is a potent inducer of this efflux transporter (12). Accordingly, premedication with dexamethasone may affect docetaxel kinetics in tumors.

The primary objective of the present study was to evaluate the feasibility of quantitative PET studies with [^{11}C]docetaxel in patients with lung cancer. As mentioned above, this required development of the optimal tracer kinetic model for quantification of [^{11}C]docetaxel kinetics in lung cancer patients and validation of the use of a noninvasive procedure to enable implementation in routine clinical practice. The secondary objective was to explore whether [^{11}C]docetaxel kinetics were associated with tumor perfusion, tumor size, and administration of premedication with dexamethasone. Finally, as a limited number of patients were actually scheduled for docetaxel therapy, a preliminary assessment of the relationship between [^{11}C]docetaxel uptake and response to docetaxel therapy was possible.

Patients and Methods

Patients

Thirty-four patients (23 males and 11 females; median age 62 years; range 32–74 years) with advanced-stage cancer were prospectively enrolled prior to planned systemic therapy. Thirty-two patients were diagnosed with non-small cell lung cancer and two with malignant mesothelioma. Criteria for enrollment in the study were 18 years of age or older, a malignant lesion of at least 1.5 cm in diameter within the chest, life expectancy of at least 12 weeks, Karnofsky performance status scale >60%, thrombocyte count $>100 \times 10^9 \cdot L^{-1}$, and hemoglobin >6.0 $mmol \cdot L^{-1}$. Exclusion criteria included previous treatment with taxanes, claustrophobia, pregnancy or lactation, metal implants (e.g., pacemakers), use of coumarin derivatives or inhibitors of thrombocyte aggregation, use of inhibitors or substrates of the efflux transporter ABCB1, concurrent treatment with experimental drugs, and participation in a clinical trial with any investigational drug within 30 days prior to study entry. When patients were scheduled for docetaxel therapy, computed tomography (CT) scans were carried out at baseline and every cycle or every two cycles of treatment to assess clinical response according to Response Evaluation Criteria in Solid Tumors (RECIST) version 1.1 (13). The study was approved by the Medical Ethics Review Committee of the VU University Medical Center. Prior to inclusion, each patient signed a protocol-specific informed consent.

Synthesis of radiopharmaceuticals

[^{15}O]H_2O and [^{11}C]docetaxel were synthesized according to Good Manufacturing Practice (GMP) standards as described previously (3, 4, 14). Docetaxel was obtained from Green PlantChem Company Ltd., which was used to synthesize the precursor of [^{11}C]docetaxel. [^{11}C]docetaxel itself was produced with a decay-corrected overall radiochemical yield of 10 ± 1% prior to purification. The median specific activity at time of injection was 2.0 $GBq \cdot \mu mol^{-1}$ (range: 1.0–37.3 $GBq \cdot \mu mol^{-1}$).

Scanning protocol

Studies were conducted on a Gemini TF-64 PET-CT scanner (Philips Medical Systems; ref. 15). This scanner has an axial field of view of 18 cm, divided into 45 contiguous planes. All patients underwent a dynamic

Downloaded from http://aacrjournals.org/clincancerres/article-pdf/17/14/4814/1997884/4814.pdf by guest on 09 October 2024

[^{11}C]docetaxel PET–CT scan. Eight patients underwent a second [^{11}C]docetaxel scan to assess test–retest reproducibility of measurements. The second [^{11}C]docetaxel scan was carried out approximately 4 hours after the first. Twenty-eight patients underwent an additional PET scan using [^{15}O]H_2O to measure tumor perfusion.

Patients were asked to fast from midnight before scanning. A light breakfast at 08.00 hours or a light lunch at 12.00 hours, and water and tea were allowed until PET scanning. In the first 24 patients, dexamethasone (8 mg p.o.) was given to prevent potential allergic reactions. As none of these patients did experience any side-effects, the Medical Ethics Review Committee allowed dexamethasone administration to be discarded in subsequent patients.

All patients received two venous catheters, one for tracer injection, the other for blood sampling. In addition, 17 patients received an indwelling radial artery catheter for arterial blood sampling during the dynamic [^{11}C]docetaxel scan. Patients were positioned supine on the scanner bed with both tumor and aortic arch located inside the axial field of view of the scanner. Elastic body-restraining bandages were used to minimize movement during scanning.

Following a 50 mAs low-dose CT scan for attenuation correction, a 10 minutes dynamic scan was started simultaneously with an intravenous injection of 370 MBq [^{15}O]H_2O (5 mL at a rate of 0.8 mL·s^{-1}), followed by a 35 mL saline flush (rate 2 mL·s^{-1}). At least 20 minutes after administration of [^{15}O]H_2O, which has a half-life of 2 minutes, a 60-minute dynamic scan was started simultaneously with an intravenous injection of [^{11}C]docetaxel (median dose 335 MBq; range 133–385 MBq; dissolved in a maximum volume of 12 mL saline, at a rate of 0.8 mL·s^{-1}), followed by 35 mL saline (rate 2 mL·s^{-1}).

Data were normalized and all appropriate corrections were applied for dead time, decay, randoms, scatter, and attenuation. Using the 3-dimensional row action maximum likelihood reconstruction algorithm (3D RAMLA), [^{15}O]H_2O and [^{11}C]docetaxel scans were reconstructed into 26 (1 × 10, 8 × 5, 4 × 10, 2 × 15, 3 × 20, 2 × 30, and 6 × 60 s) and 36 (1 × 10, 8 × 5, 4 × 10, 2 × 15, 3 × 20, 2 × 30, 6 × 60, 4 × 150, 4 × 300, and 2 × 600 s) frames, respectively.

Blood sampling

In the first 17 patients, arterial blood sampling was carried out during [^{11}C]docetaxel scanning. Using an online detection system (16), arterial blood was withdrawn continuously at a rate of 5 mL·min^{-1} during the first 5 minutes and 1.7 mL·min^{-1} thereafter. Twenty-nine minutes after injection, online sampling was discontinued to minimize the total amount of blood to be taken. In addition, both 10 mL arterial and venous samples were collected manually at 2.5, 5, 10, 15, 20, 30, 40, and 60 minutes postinjection. Prior to each sample, 3–5 mL blood was discarded and the line was flushed with 2 mL saline after each sample. Blood samples were analyzed for blood and plasma concentrations and potential radiolabeled metabolites of [^{11}C]docetaxel as described in the Supplementary Data.

Input functions

Blood sampler data of [^{11}C]docetaxel were corrected for delay relative to the time-activity curve of the ascending aorta. The resulting delay-corrected sampler curve was calibrated using the manually drawn arterial blood samples. Plasma/whole blood ratios derived from the manual blood samples were fitted to a sigmoid function. Finally, the blood sampler input function (BSIF) was obtained by multiplying the delay-corrected and calibrated sampler curve with this sigmoid function.

IDIFs were derived for both [^{15}O]H_2O and [^{11}C]docetaxel scans. An IDIF of the ascending aorta has been validated for several PET tracers including [^{15}O]H_2O (17) and it is considered to be a noninvasive alternative to arterial sampling. Hence, volumes of interest (VOI) of 1 cm diameter were drawn over the ascending aorta in approximately 10 consecutive image planes of the frame in which the first pass of the bolus was best visualized. Projection of these VOIs onto all image frames yielded the arterial time-activity curve $C_A(t)$. A similar approach was used for right ventricular cavity and pulmonary artery, thereby providing a time-activity curve for the pulmonary circulation $C_V(t)$ (17). For [^{11}C]docetaxel, the plasma IDIF was obtained by multiplying $C_A(t)$ with a sigmoid function describing the plasma/whole blood ratio over time. The correction for plasma/whole blood ratio was based on either arterial or venous sampling.

Delineation of tumors

Tumors were defined on the low-dose CT scans by an experienced nuclear medicine physician (E.F.C.) who was blinded to patients' history and outcome. To this end, all low-dose CT images were converted to ECAT 7 format and tumor VOIs were drawn using the CAPP software package (CTI/Siemens). Finally, these VOIs were projected onto the dynamic images of the corresponding [^{15}O]H_2O and [^{11}C]docetaxel scans, thereby generating tumor time-activity curves for [^{15}O]H_2O and [^{11}C]docetaxel.

Analysis of tumor perfusion

Kinetic analysis of data was carried out using dedicated programs written within the software environment Matlab (The MathWorks Inc.). The standard single-tissue compartment model was used to derive tumor perfusion from [^{15}O]H_2O kinetics, applying corrections for both arterial and pulmonary artery blood volume (18):

$$C_T(t) = (1 - V_A - V_V) \cdot F \cdot C_A(t) \otimes e^{-\frac{F}{V_T}t} + V_A C_A(t) + V_V C_V(t)$$

where $C_T(t)$ represents measured tissue [^{15}O]H_2O concentration as function of time, F perfusion, V_A arterial blood volume, V_V pulmonary circulation blood volume, and V_T the volume of distribution or partition coefficient of water.

Using nonlinear regression, tumor time-activity curves were fitted to this single-tissue compartment model using

Downloaded from http://aacrjournals.org/clincancerres/article-pdf/17/14/4814/1997884/4814.pdf by guest on 09 October 2024

IDIF as arterial input function (17). The correction for pulmonary circulation blood volume was included, as it improved the quality of the fits without affecting tumor perfusion values (17).

Analysis of [^{11}C]docetaxel kinetics in tumors

To develop a kinetic model and validate the use of a noninvasive procedure for quantification of [^{11}C]docetaxel data, only lesions with a volume $\geq$4 cm^3 were considered.

The generated time-activity curves of arterial blood and tumor tissue were entered into the analysis (Fig. 1). First, nonlinear regression analysis was applied to fit the tumor time-activity curves of [^{11}C]docetaxel to a two-tissue reversible (4 rate constants) and a two-tissue irreversible (3 rate constants) compartment model, both including a blood volume parameter and using the BSIF derived plasma input function. Akaike and Schwarz criteria (19, 20) were used to determine which model best described [^{11}C]docetaxel kinetics in tumors.

The two-tissue compartment model (Fig. 1) describes the total tissue signal (C_T) by the following equation:

$$C_T(t) = C_1(t) + C_2(t)$$

where $C_1(t)$ and $C_2(t)$ are concentrations in 1st and 2nd compartment, respectively. Kinetics in both compartments are given by the following differential equations:

$$\frac{dC_1(t)}{dt} = K_1 C_p(t) - (k_2 + k_3)C_1(t) + k_4 C_2(t)$$

$$\frac{dC_2(t)}{dt} = k_3 C_1(t) - k_4 C_2(t)$$

where C_P is arterial plasma concentration, K_1 the rate constant for transport from plasma to tumor, k_2 the rate

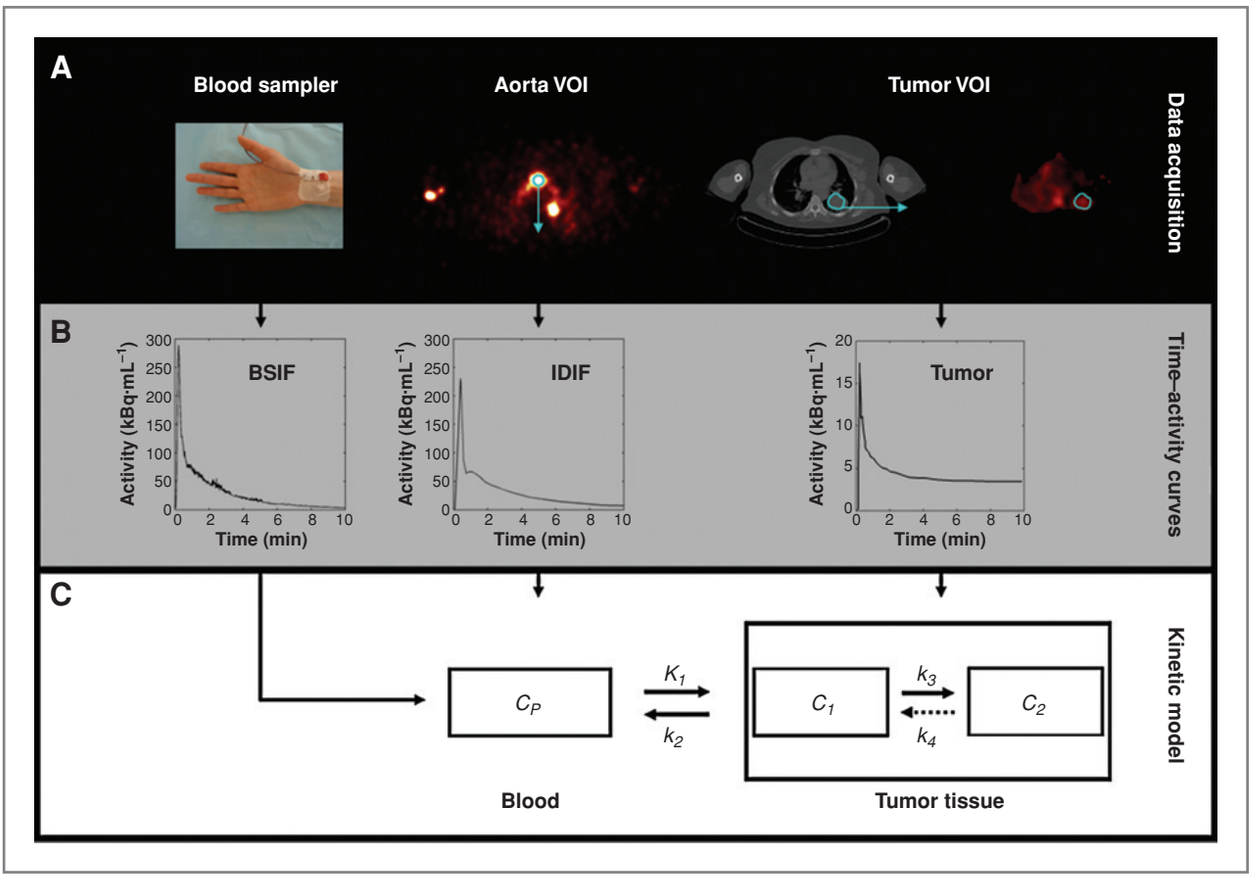

Figure 1. Compartmental modeling of dynamic [^{11}C]docetaxel PET scans. A, arterial concentrations of [^{11}C]docetaxel were obtained from arterial blood sampling or an IDIF. For the latter, VOIs were drawn over the ascending aorta in a frame in which the first pass of the bolus was best visualized. In addition, a tumor VOI was defined on the low-dose CT scan. Finally, aorta VOI and tumor VOI were projected onto the dynamic images of the corresponding [^{11}C]docetaxel scan, thereby generating time-activity curves. B, time-activity curves of arterial blood and tumor tissue were entered into two-tissue compartment modeling. To this end, either BSIF or IDIF was entered into the analysis as arterial input function. C, schematic diagram of a two-tissue compartment model. The concentration (C) in the tumor consists of [^{11}C]docetaxel in compartments 1 (C_1) and 2 (C_2), representing free and bound [^{11}C]docetaxel, respectively. Kinetics of [^{11}C]docetaxel in tumor tissue is regulated by input from plasma (C_P) and four kinetic rate constants K_1, k_2, k_3, and k_4. K_1 is the rate constant describing transport from plasma to tumor, k_2 is the rate constant for clearance from tumor to plasma, and k_3 and k_4 are kinetic rate constants describing exchange between the two tumor compartments. For the irreversible two-tissue compartment model $k_4 = 0$. VOI, volume of interest; BSIF, blood sampler derived input function; IDIF, image derived input function.

Downloaded from http://aacrjournals.org/clincancerres/article-pdf/17/14/4814/1997884/4814.pdf by guest on 09 October 2024

constant for clearance from tumor to plasma, and k_3 and k_4 kinetic rate constants describing exchange between 1st and 2nd compartment.

For the irreversible two-tissue compartment model, k_4 is 0. In this case the net influx rate constant K_i can be calculated:

$$K_i = \frac{K_1 \cdot k_3}{k_2 + k_3}.$$

In case of irreversible uptake, both robustness and simplicity of the K_i estimation can be improved by using the Patlak method (21). The Patlak plot is a linearization of the compartmental equations, and is given by:

$$\frac{C_T(t)}{C_p(t)} = K_i \cdot \frac{\int_0^t C_p(\tau) \cdot d\tau}{C_p(t)} + V_0,$$

where the intercept V_0 represents the initial volume of distribution. K_i is now given by the slope of the linear part of the curve.

The schematic diagram in Supplementary Fig. S1 illustrates the various steps that were carried out to develop a simplified procedure suitable for clinical implementation of [^{11}C]docetaxel studies. After validation of a simplified kinetic analysis (i.e., Patlak analysis), use of IDIF was compared with use of BSIF. Next, the use of discrete venous rather than arterial samples to correct IDIF for the time course of the plasma/whole blood ratio was investigated. Finally, the least invasive procedure was used to determine test–retest variability of [^{11}C]docetaxel quantification in tumors.

[^{11}C]docetaxel clearance

To determine the effect of dexamethasone on blood kinetics of [^{11}C]docetaxel, the clearance of [^{11}C]docetaxel was calculated using the following equation:

$$\text{Clearance} = \frac{D}{\int C_p(t) \cdot dt \cdot BSA}$$

where the injected does (D) of [^{11}C]docetaxel is divided by the integral of the plasma time-activity curve multiplied by the body-surface area (BSA).

Statistics

Statistical analysis was carried out using SPSS software (SPSS for Windows 16.0, SPSS, Inc.). Correlations were explored using the Spearman's correlation coefficient. Level of agreement was assessed using the intraclass correlation coefficient with a 2-way random model and Bland–Altman analysis (22). The Mann–Whitney test was used to compare between groups.

Results

[^{11}C]docetaxel kinetics in blood

Initially, the plasma/whole blood ratio was >1, but it rapidly decreased to values <1 from 15 minutes onward (Supplementary Fig. S2A). There was high correlation between plasma/whole blood ratios obtained from arterial and venous sampling (Spearman's $\rho = 0.970$; $P < 0.001$; $n = 169$). In all patients, there was rapid systemic clearance

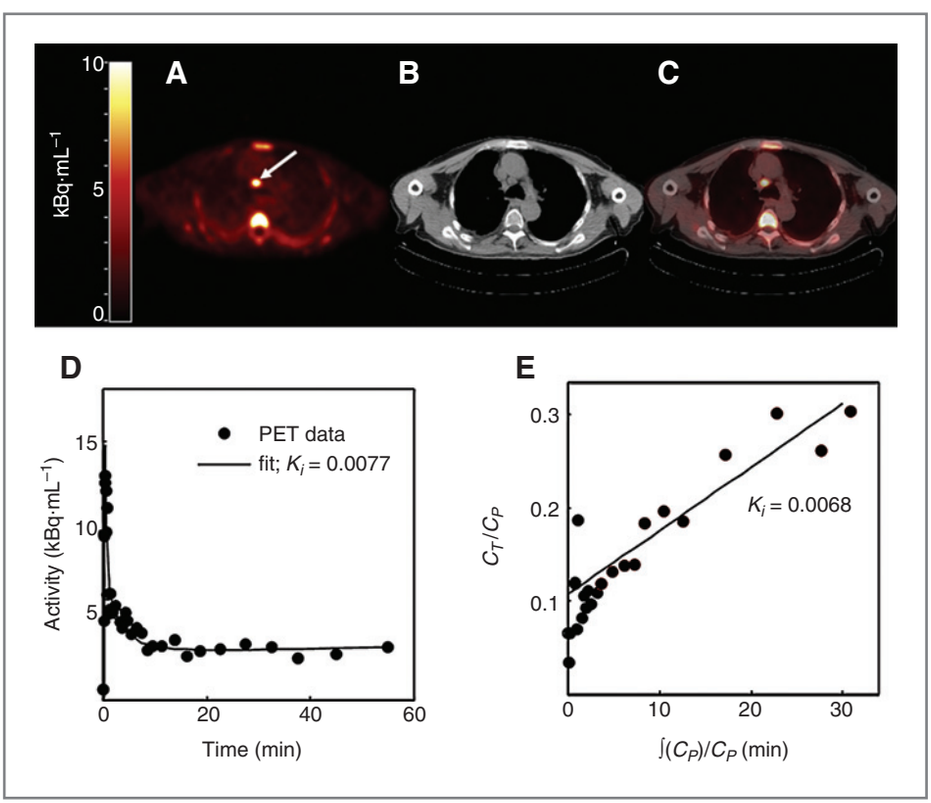

Figure 2. A, PET image of [^{11}C]docetaxel uptake at 10–60 minutes post injection showing a mediastinal metastasis with increased [^{11}C]docetaxel uptake (arrow). B, corresponding CT image. C, PET-CT fusion image. D, representative time-activity curve in the corresponding tumor. E, Patlak-plot of [^{11}C]docetaxel in the corresponding tumor. K_i, net influx rate constant; C_T, measured PET activity in tumor; C_P, measured plasma activity in arterial blood.

Downloaded from http://aacrjournals.org/clincancerres/article-pdf/17/14/4814/1997884/4814.pdf by guest on 09 October 2024

of radioactivity from blood (Supplementary Fig. S2B). This precluded reliable high performance liquid chromatography (HPLC) measurements of radiolabeled metabolites of [11C]docetaxel beyond 15 minutes after injection. Over the first 15 minutes, HPLC chromatograms did not reveal any radiolabeled metabolites and no radioactivity was measured in the solid-phase-extraction-rinsing fraction. Due to this rapid clearance of [11C]docetaxel, calibration of the BSIF was not reliable at time points > 10 minutes after injection. Therefore, only the first 10 minutes of data were used for further analysis.

Quantification of [11C]docetaxel kinetics in tumors

[11C]docetaxel accumulated in lung cancer lesions (Fig. 2). Fig. 2D shows a representative time-activity curve of [11C]docetaxel in lung cancer. In the 17 patients who underwent arterial blood sampling, a total of 15 lesions had a volume $\geq$4 cm^3. As a result, 15 lesions were eligible for validation of a simplified method for the analysis of [11C]docetaxel PET/CT scans. According to both Akaike and Schwarz criteria, the irreversible two-tissue compartment model was the kinetic model of choice for 14 out of 15 lesions.

The irreversible behavior of [11C]docetaxel kinetics was confirmed by Patlak plots, which became linear soon after injection (Fig. 2E). The Patlak method showed the most robust values for K_i, whereas the individual microparameters K_1, k_2, and k_3 showed relative large standard errors, which are due to noise levels of tissue tracer kinetics.

Validation of a less invasive procedure

Patlak and nonlinear regression analyses of [11C]docetaxel data produced comparable K_i values (Spearman's $\rho = 0.979$; $P < 0.001$; Fig. 3A). Therefore, the more robust and faster Patlak method was used in further analyses. Although K_i values were lower for ascending aorta derived IDIF than those for corresponding BSIF (Fig. 3B), correlation between both sets of K_i values was high (Spearman's $\rho = 0.946$; $P < 0.001$). Use of venous and arterial samples to correct IDIF for plasma/whole blood ratios resulted in comparable K_i values (Spearman's $\rho = 0.986$; $P < 0.001$; Fig. 3C). According to the Patlak method, the median K_i values were 0.011 mL·cm^{-3}·min^{-1} (range, 0.003–0.024 mL·cm^{-3}·min^{-1}), 0.008 mL·cm^{-3}·min^{-1} (range, 0.003–0.019 mL·cm^{-3}·min^{-1}), and 0.008 mL·cm^{-3}·min^{-1} (range, 0.003–0.021 mL·cm^{-3}·min^{-1}) for BSIF, IDIF using arterial samples and IDIF using venous samples, respectively.

Finally, using IDIF (with plasma/whole blood corrections based on venous samples) in the test–retest analysis showed good reproducibility for K_i (Fig. 3D) with an intraclass correlation coefficient of 0.952 (95% confidence interval: 0.781–0.990), an absolute repeatability coefficient of 0.003 mL·cm^{-3}·min^{-1} and a relative repeatability coefficient of 29%. These results indicate that an IDIF, together with venous blood samples, could be used as a noninvasive arterial input function. Consequently, arterial sampling could be discarded in the following patients. Finally, venous samples were used to quantify tumor uptake of [11C]docetaxel in all 34 patients.

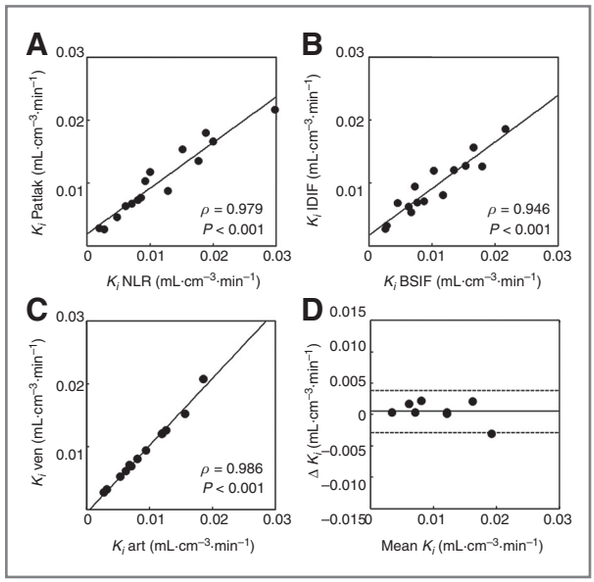

Figure 3. Plots showing the essential results of the subsequent validation steps indicated in Supplementary Fig. S1. A, Spearman's correlation between Patlak derived K_i and NLR derived K_i with plasma input function obtained from BSIF. B, Spearman's correlation between IDIF derived K_i and BSIF derived K_i; in both cases K_i was calculated using the Patlak method and arterial samples were used to correct the input function for changing plasma/whole blood ratios. C, Spearman's correlation between Patlak derived K_i using venous samples and Patlak derived K_i using arterial samples, where IDIF was corrected for changing plasma/whole blood ratios using either arterial samples or venous samples. D, Bland–Altman plot of Patlak derived K_i test–retest data, where IDIF was corrected for changing plasma/whole blood ratios using venous samples. Dotted lines represent $\pm$1.96 $\times$ SD values. K_i, net influx rate constant; NLR, nonlinear regression; ρ, Spearman's correlation coefficient; P, P-value; IDIF, image derived input function; BSIF, blood sampler input function; art, arterial samples; ven, venous samples; solid lines (A–C) represent linear fits through the data points; mean K_i, mean K_i of test and retest scans; ΔK_i, absolute difference in K_i between test and retest scans.

Correlation with tumor perfusion

In the 28 patients who underwent an additional PET scan with [15O]H_2O, a total of 27 lesions (20 primary tumors and 7 metastases) with a size $\geq$4 cm^3 could be defined on the low-dose CT scan. In these lesions, tumor perfusion was variable with a median perfusion of 0.281 mL·cm^{-3}·min^{-1} (range, 0.052–0.904 mL·cm^{-3}·min^{-1}). A significant association between K_i of [11C]docetaxel and tumor perfusion was found (Spearman's $\rho = 0.815$; $P < 0.001$; Fig. 4).

Correlation with tumor size

Overall, 32 lesions (22 primary tumors and 10 metastases) could be identified on the corresponding low-dose CT scans. In these lesions, the K_i of [11C]docetaxel was variable (range, 0.0023–0.0229 mL·cm^{-3}·min^{-1}) with a median K_i of 0.0092 mL·cm^{-3}·min^{-1}. Although the size of the lesions was highly variable (median size, 20 cm^3; range, 5–485 cm^3), there was no association between tumor

Downloaded from http://aacrjournals.org/clincancerres/article-pdf/17/14/4814/1997884/4814.pdf by guest on 09 October 2024

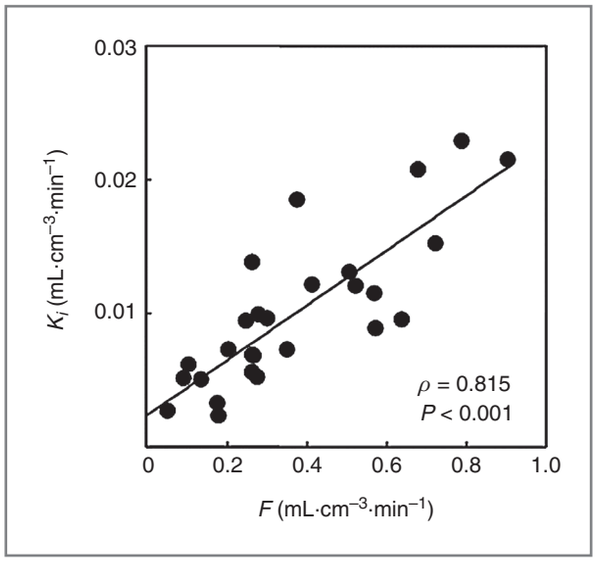

Figure 4. Net influx rate constant of [^{11}C]docetaxel *versus* tumor perfusion. The solid line represents the linear least squares fit through the measured data. K_i, net influx rate constant; F, tumor perfusion; ρ, Spearman's correlation coefficient; P, P-value.

size and K_i of [^{11}C]docetaxel (Spearman's $\rho = -0.140$; $P = 0.446$) or tumor perfusion (Spearman's $\rho = -0.139$; $P = 0.491$).

Effects of dexamethasone on [^{11}C]docetaxel kinetics

As premedication with dexamethasone was required in the first 24 patients and discontinued thereafter, it was possible to investigate potential effects of dexamethasone administration on [^{11}C]docetaxel kinetics in tumors (size $\geq$4 cm^3). Dexamethasone treated patients had significantly lower K_i values (median K_i, 0.0072 mL·cm^{-3}·min^{-1}; range, 0.0023–0.0208 mL·cm^{-3}·min^{-1}) than patients not pretreated with dexamethasone (median K_i, 0.0118 mL·cm^{-3}·min^{-1}; range, 0.0051–0.0229 mL·cm^{-3}·min^{-1}; Mann–Whitney, $P = 0.013$; Fig. 5A).

Although tumor perfusion was somewhat lower in patients pretreated with dexamethasone (median perfusion, 0.265 mL·cm^{-3}·min^{-1}; range, 0.052–0.725 mL·cm^{-3}·min^{-1}) as compared with patients who were not pretreated with dexamethasone (median perfusion, 0.396 mL·cm^{-3}·min^{-1}; range, 0.093–0.904 mL·cm^{-3}·min^{-1}), this difference did not reach statistical significance (Mann–Whitney, $P = 0.093$; Fig. 5B). However, when K_i was normalized for tumor perfusion, there was no difference between patients who were pretreated with dexamethasone and patients who were not pretreated (Mann–Whitney, $P = 0.297$). When analyzed separately, the association between K_i of [^{11}C]docetaxel and tumor perfusion still persisted in both patients treated (Spearman's $\rho = 0.785$; $P = 0.001$) and not treated (Spearman's $\rho = 0.552$; $P = 0.063$) with dexamethasone. Furthermore, dexamethasone administration did not affect [^{11}C]docetaxel clearance from plasma. The median plasma clearance during the first 10 minutes of data was 8.24 mL·s^{-1}·m^{-2} (range, 6.09–12.40 mL·s^{-1}·m^{-2}) and 8.27 mL·s^{-1}·m^{-2} (range, 6.32–9.44 mL·s^{-1}·m^{-2}) in patients with and without dexamethasone premedication, respectively (Mann–Whitney, $P = 0.724$; Fig. 5C).

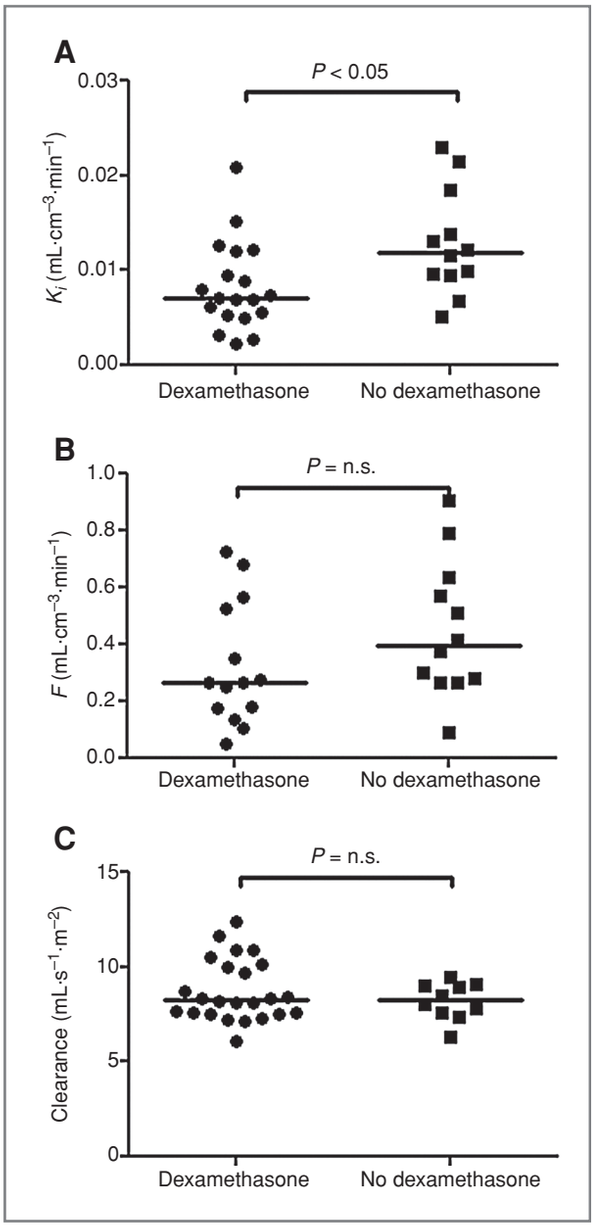

Figure 5. Comparison of results for patients with and without dexamethasone pretreatment. A, K_i of [^{11}C]docetaxel in tumors. B, Tumor perfusion. C, Plasma clearance of [^{11}C]docetaxel. K_i, net influx rate constant; F, tumor perfusion; n.s. not significant.

[^{11}C]docetaxel kinetics and clinical outcome

Seven non-small cell lung cancer patients were scheduled for docetaxel therapy following this PET study. Three of those were treated simultaneously with platinum-based agents. All patients received premedication with

Downloaded from http://aacrjournals.org/clincancerres/article-pdf/17/14/4814/1997884/4814.pdf by guest on 09 October 2024

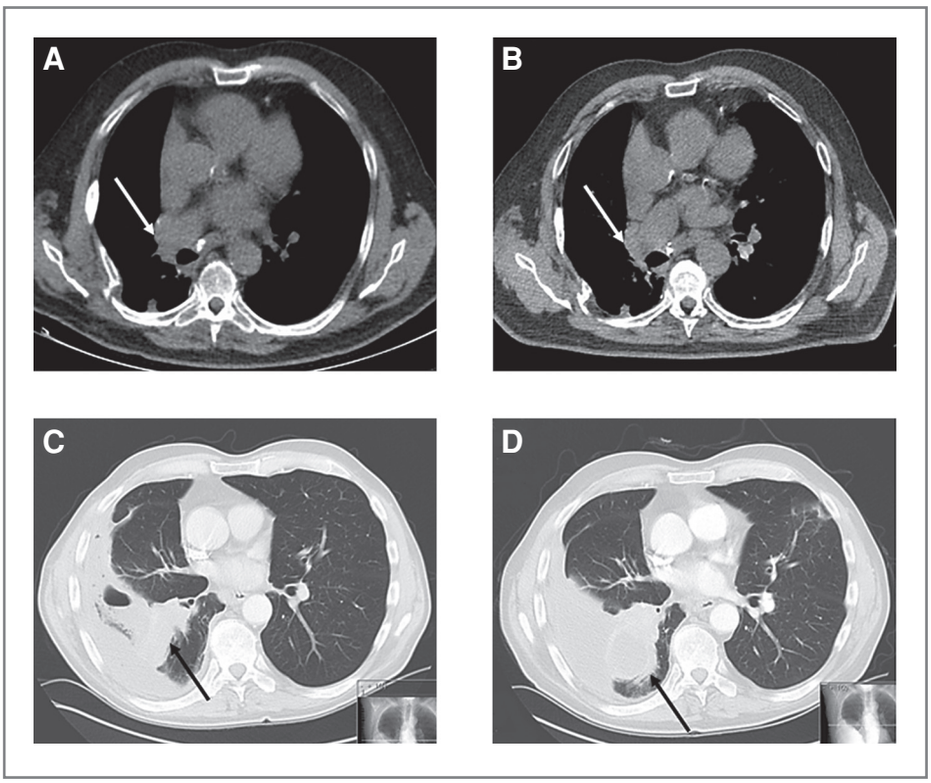

Figure 6. Computed tomography images of 2 patients with metastatic non-small cell lung cancer who were treated with docetaxel. A–B, example of a patient with relatively high [^{11}C]docetaxel uptake (K_i = 0.0151 mL·cm^{-3}·min^{-1}) in recurrent disease (arrow), which showed stable disease (B) as compared with baseline (A). C–D, example of a patient with relatively low [^{11}C]docetaxel uptake (K_i = 0.0050 mL·cm^{-3}·min^{-1}) in the primary tumor (arrow), which showed rapid progression with increased atelectasis within 2 months (D) as compared with baseline (C).

dexamethasone prior to PET scanning. When smaller tumors were also included, a total of 12 lesions could be identified in the field of view of the PET scan. In these lesions, the median tumor size was 3 cm^3 (range, 1–334 cm^3) with a median [^{11}C]docetaxel K_i of 0.0073 mL·cm^{-3}·min^{-1} (range, 0.0023–0.0228 mL·cm^{-3}·min^{-1}). In the first evaluation, the median change in the longest diameter of these lesions was 4% (range, −6% to 100%). The K_i of [^{11}C]docetaxel was negatively associated with the change in tumor size (Spearman's $\rho = -0.803$; $P = 0.002$). Tumors with a K_i value > 0.0073 mL·cm^{-3}·min^{-1} had a significantly better response than tumors with a lower K_i value (Mann–Whitney, $P = 0.007$). Figure 6 shows an example of a patient with stable disease and another patient with progressive disease. The change in tumor size was not significantly affected by additional treatment with platinum-based agents (Mann–Whitney, $P = 0.073$).

Discussion

Docetaxel is an effective drug for the treatment of patients with several cancers, including non-small cell lung cancer (23, 24). However, tumor resistance to docetaxel therapy remains a major challenge. Quantitative [^{11}C]docetaxel PET studies may provide insight in kinetics of docetaxel in tumors and therefore contribute to appropriate selection of cancer patients for docetaxel therapy. Using a state of the art validation approach, the present study shows the feasibility and reproducibility of quantitative PET studies with [^{11}C]docetaxel in patients with lung cancer. Tumor kinetics of [^{11}C]docetaxel were irreversible and associated with tumor perfusion. Patients pretreated with dexamethasone showed significantly lower [^{11}C]docetaxel uptake in tumors, whereas no difference in [^{11}C]docetaxel clearance was measured in these patients. In the few patients who were subsequently treated with docetaxel, [^{11}C]docetaxel uptake in tumors seemed to be associated with treatment outcome.

[^{11}C]docetaxel showed fast kinetics, reflected by the rapid clearance of radioactivity from blood. Consequently, only 10 minutes of blood data could be used, as input functions were not reliable at later times. In addition, 10–15 minutes after injection already more than 50% of the total administered activity was located in the liver. Rapid clearance of [^{11}C]docetaxel from blood and high [^{11}C]docetaxel uptake in liver likely reflect extensive metabolism of docetaxel. Nevertheless, no radiolabeled metabolites of [^{11}C]docetaxel were detected, obviating the need to correct the arterial input function for radiolabeled metabolites. In the liver microsomes, docetaxel is metabolized mainly by the cytochrome P450 enzyme CYP3A4 (25). Hepatic transformation and subsequent biliary excretion into feces is known to account for ~80% of the elimination of an administered therapeutic dose (26). In addition, active efflux by ABCB1 in intestine and biliary system represents an alternative pathway of docetaxel elimination (27).

K_i of [^{11}C]docetaxel in lung cancer was variable and highly related to tumor perfusion, but not to tumor size.

Downloaded from http://aacrjournals.org/clincancerres/article-pdf/17/14/4814/1997884/4814.pdf by guest on 09 October 2024

Tumor perfusion also was variable, which may reflect interindividual differences in tumor vasculature. The tumor vasculature itself may also limit [^{11}C]docetaxel delivery to tumors, as it is structurally and functionally abnormal, consisting of leaky and dilated vessels that result in increased interstitial fluid pressure and reduced drug penetration (28). Limited drug penetration in tumors is an important mechanism of tumor resistance to docetaxel therapy. A previous study in tumor xenografts showed that docetaxel accumulation was limited to the first ~100 μm around a blood vessel, with little drug reaching a distance of 100 to 150 μm (29). Although a larger tumor size may result in reduced perfusion in the central part, consequently leading to lower average perfusion values, no associations between tumor size and [^{11}C]docetaxel kinetics or tumor perfusion were found.

The high correlation between tumor perfusion and [^{11}C]docetaxel uptake suggests that tumor uptake of [^{11}C]docetaxel primarily depends on tumor perfusion. Consequently, administration of drugs that change tumor perfusion, e.g., antiangiogenic agents, may have significant effects on docetaxel delivery to tumors, possibly affecting its efficacy. The methodology developed here, measuring both perfusion and docetaxel kinetics, provides a noninvasive means to investigate effects of antiangiogenic drugs on both tumor perfusion and docetaxel delivery. This, in turn, may lead to optimized scheduling of drugs, thereby enhancing antitumor efficacy of combination therapy.

Next to tumor perfusion, intracellular binding of [^{11}C]docetaxel to tubulin may determine [^{11}C]docetaxel kinetics in tumors. The taxane docetaxel acts by binding to the beta-tubulin subunit of the microtubules, promoting tubulin assembly into microtubules, stabilizing them, and inhibiting depolymerization to free tubulin (2). Tumor cells can alter the tubulin isotype, thereby reducing docetaxel binding (30) with subsequent lower K_i values of [^{11}C]docetaxel.

Apart from those parameters that regulate uptake of [^{11}C]docetaxel in tumor tissue, efflux from tumor cells may be another determinant of [^{11}C]docetaxel kinetics, especially because docetaxel is a substrate for the drug efflux transporter ABCB1 (9). This efflux transporter is a member of the ATP binding cassette family and may contribute to multidrug resistance in tumors by actively eliminating drugs from cancer cells (31). The lower K_i values of [^{11}C]docetaxel measured in patients treated with the ABCB1 inducer dexamethasone may reflect the importance of ABCB1 for [^{11}C]docetaxel kinetics in tumors. In addition, antivascular effects of dexamethasone may contribute to the lower K_i values of [^{11}C]docetaxel, because dexamethasone is known to decrease total blood volume in tumors (32). The nonsignificant difference in perfusion-normalized K_i values suggests that reduced tumor perfusion may contribute to lower [^{11}C]docetaxel uptake in dexamethasone pretreated patients. Although dexamethasone potentially increases [^{11}C]docetaxel clearance by inducing both intestinal ABCB1 (12) and CYP3A4 activity (33), dexamethasone administration was not associated with higher [^{11}C]docetaxel plasma clearance. As calculated K_i values of [^{11}C]docetaxel were corrected for the activity in plasma, the present explorative analysis suggests that dexamethasone may affect [^{11}C]docetaxel kinetics in tumors. To date, conflicting results have been reported on the antitumor effects of dexamethasone in addition to docetaxel (34, 35). Because dexamethasone is administered routinely as premedication for docetaxel, more studies are required to further clarify the effects of dexamethasone and its scheduling on perfusion and docetaxel kinetics in tumors.

PET using radiolabeled anticancer drugs may be valuable for predicting outcome prior to start of treatment and, as such, it may be an important tool for individualized treatment planning. Human PET studies with radiolabeled anticancer drugs (36), including F-18 labeled 5-fluorouracil ([^{18}F]5-FU; ref 37 and 38) and tamoxifen ([^{18}F]fluorotamoxifen; ref. 39), have shown that high tumor concentrations of the radiolabeled drug were associated with improved tumor response. Although the present study was not designed to predict tumor response to docetaxel therapy, the finding in the limited number of docetaxel-treated patients suggests that variable [^{11}C]docetaxel kinetics in tumors may reflect differential sensitivity to docetaxel therapy. Ideally, only patients scheduled for docetaxel treatment should have been selected for the present study. In the present validation study, however, three cannulas including one for arterial sampling were required and therefore also patients scheduled for other therapies were included. The noninvasive approach developed in this study now provides a means to investigate the relationship between [^{11}C]docetaxel uptake and response to docetaxel treatment in larger cohorts of lung cancer patients and in patients with other tumors located in the thoracic region such as locally advanced breast cancer. Although microdosing prevents patients from drug-induced toxicities associated with therapeutic doses, it has potential limitations, as the kinetic behavior of tracer and therapeutic doses differ. Therefore, further PET studies using [^{11}C]docetaxel during docetaxel therapy are also needed to assess whether tumor kinetics are dose dependent.

In conclusion, full quantification of [^{11}C]docetaxel kinetics in lung cancer patients using a noninvasive PET based approach is feasible. Tumor kinetics of [^{11}C]docetaxel were highly variable and strongly related to tumor perfusion. In addition, uptake of [^{11}C]docetaxel in tumors was reduced in patients pretreated with dexamethasone. Variable [^{11}C]docetaxel kinetics in tumors may reflect differential sensitivity to docetaxel therapy. The findings of this study warrant further clinical studies investigating the predictive value of initial [^{11}C]docetaxel uptake and the effects of comedication on docetaxel kinetics in tumors.

Disclosure of Potential Conflicts of Interest

No potential conflicts of interest were disclosed.

Downloaded from http://aacrjournals.org/clincancerres/article-pdf/17/14/4814/1997884/4814.pdf by guest on 09 October 2024

Acknowledgments

The authors would like to thank Suzette van Balen, Amina Elouahmani, Judith van Es, Robin Hemminga, Femke Jongsma, Rob Koopmans, Nghi Pham, Nasserah Sais, Annemiek Stiekema, and Jeroen Wilhelmus for scanning the patients, Niki Hoetjes, Marc Huisman, Jurgen Mourik, and Floris van Velden for help with processing of the blood samples, Otto Hoekstra, Natasja Kok, Daniela Oprea-Lager, Ilona Pomstra, Pieter Raijmakers, and Atie van Wijk for help with logistic planning and patient care, Pieter Postmus and Hugo Rutten for recruiting patients, Dennis Boersma for technical assistance, Ronald Boellaard for help with data analysis, Stefan de Haan and Sebastiaan Kleijn for assistance with the Figures, Jonas Eriksson, Rob Klok, and Dennis Laan for the production of [^{11}C]docetaxel, Gert Luurtsema, Marissa Rongen, and Kevin Takkenkamp for the production of [^{15}O]H_2O and the analysis of the blood samples.

Grant Support

This study was financially supported by VUmc Cancer Center Amsterdam.

The costs of publication of this article were defrayed in part by the payment of page charges. This article must therefore be hereby marked *advertisement* in accordance with 18 U.S.C. Section 1734 solely to indicate this fact.

Received November 3, 2010; revised April 23, 2011; accepted May 16, 2011; published OnlineFirst July 12, 2011.

References

1. Ganansia-Leymarie V, Bischoff P, Bergerat JP, Holl V. Signal transduction pathways of taxanes-induced apoptosis. Curr Med Chem Anticancer Agents 2003;3:291–306.
2. Montero A, Fossella F, Hortobagyi G, Valero V. Docetaxel for treatment of solid tumours: a systematic review of clinical data. Lancet Oncol 2005;6:229–39.
3. Van Tilburg EW, Franssen EJ, Van der Hoeven JJ, et al. Radiosynthesis of [11C]docetaxel. J Label Compd Radiopharm 2004;47: 763–77.
4. Van Tilburg EW, Mooijer MP, Brinkhorst J, Van der Meij M, Windhorst AD. Improved and semi-automated GMP-compliant radiosynthesis of [11C]docetaxel. Appl Radiat Isot 2008;66:1414–8.
5. Van der Veldt AA, Lammertsma AA, Hendrikse NH. [11C]docetaxel and positron emission tomography for noninvasive measurements of docetaxel kinetics. Clin Cancer Res 2007;13:7522–3.
6. Van der Veldt AA, Hendrikse NH, Smit EF, Mooijer MP, Rijnders AY, Gerritsen WR, et al. Biodistribution and radiation dosimetry of ^{11}C-labeled docetaxel in cancer patients. Eur J Nucl Med 2010;37:1950–8.
7. Hoekstra CJ, Stroobants SG, Hoekstra OS, Smit EF, Vansteenkiste JF, Lammertsma AA. Measurement of perfusion in stage IIIA-N2 non-small cell lung cancer using H(2)(15)O and positron emission tomography. Clin Cancer Res 2002;8:2109–15.
8. Ramanujan S, Koenig GC, Padera TP, Stoll BR, Jain RK. Local imbalance of proangiogenic and antiangiogenic factors: a potential mechanism of focal necrosis and dormancy in tumors. Cancer Res 2000;60:1442–8.
9. Shirakawa K, Takara K, Tanigawara Y, Aoyama N, Kasuga M, Komada F, et al. Interaction of docetaxel ("Taxotere") with human P-glycoprotein. Jpn J Cancer Res 1999;90:1380–6.
10. Latreille J, Gelmon KA, Hirsh V, Laberge F, Maksymiuk AW, Shepherd FA, et al. Phase II trial of docetaxel with dexamethasone premedication in patients with advanced non-small cell lung cancer: the Canadian experience. Invest New Drugs 1999;16:265–70.
11. Piccart MJ, Klijn J, Paridaens R, Nooij M, Mauriac L, Coleman R, et al. Corticosteroids significantly delay the onset of docetaxel-induced fluid retention: final results of a randomized study of the European Organization for Research and Treatment of Cancer Investigational Drug Branch for Breast Cancer. J Clin Oncol 1997;15:3149–55.
12. Salphati L, Benet LZ. Modulation of P-glycoprotein expression by cytochrome P450 3A inducers in male and female rat livers. Biochem Pharmacol 1998;55:387–95.
13. Eisenhauer EA, Therasse P, Bogaerts J, Schwartz LH, Sargent D, Ford R, et al. New response evaluation criteria in solid tumours: revised RECIST guideline (version 1.1). Eur J Cancer 2009;45:228–47.
14. Jackson JR, Dembowski BS, Ehrenkaufer RL, McIntyre E, Reivich M. [15O]H2O, [15O]O2 and [15O]CO gas production, monitoring and quality control system. Appl Radiat Isot 1993;44:631–4.
15. Surti S, Kuhn A, Werner ME, Perkins AE, Kolthammer J, Karp JS. Performance of Philips Gemini TF PET/CT scanner with special consideration for its time-of-flight imaging capabilities. J Nucl Med 2007;48:471–80.
16. Boellaard R, Van Lingen A, Van Balen SC, Hoving BG, Lammertsma AA. Characteristics of a new fully programmable blood sampling device for monitoring blood radioactivity during PET. Eur J Nucl Med 2001;28:81–9.
17. Van der Veldt AA, Hendrikse NH, Harms H, Comans EF, Postmus PE, Smit EF, et al. Quantitative parametric perfusion images using oxygen-15 labeled water and a clinical PET-CT scanner: test-retest variability in lung cancer. J Nucl Med 2010;51:1684–90.
18. Hermansen F, Rosen SD, Fath-Ordoubadi F, Kooner JS, Clark JC, Camici PG, et al. Measurement of myocardial blood flow with oxygen-15 labelled water: comparison of different administration protocols. Eur J Nucl Med 1998;25:751–9.
19. Akaike H. A new look at the statistical model identification. IEEE Trans Autom Control 1974;19:716–23.
20. Schwarz G. Estimating the dimension of a model. Ann Statist 1978;461–4.
21. Patlak CS, Blasberg RG, Fenstermacher JD. Graphical evaluation of blood-to-brain transfer constants from multiple-time uptake data. J Cereb Blood Flow Metab 1983;3:1–7.
22. Bland JM, Altman DG. Statistical methods for assessing agreement between two methods of clinical measurement. Lancet 1986;1:307–10.
23. Kudoh S, Takeda K, Nakagawa K, Takada M, Katakami N, Matsui K, et al. Phase III study of docetaxel compared with vinorelbine in elderly patients with advanced non-small-cell lung cancer: results of the West Japan Thoracic Oncology Group Trial (WJTOG 9904). J Clin Oncol 2006;24:3657–63.
24. Shepherd FA, Dancey J, Ramlau R, Mattson K, Gralla R, O'Rourke M, et al. Prospective randomized trial of docetaxel versus best supportive care in patients with non-small-cell lung cancer previously treated with platinum-based chemotherapy. J Clin Oncol 2000;18:2095–103.
25. Marre F, Sanderink GJ, De Sousa G, Gaillard C, Martinet M, Rahmani R. Hepatic biotransformation of docetaxel (Taxotere) in vitro: involvement of the CYP3A subfamily in humans. Cancer Res 1996;56: 1296–302.
26. Clarke SJ, Rivory LP. Clinical pharmacokinetis of docetaxel. Clin Pharmacokinet 1999;36:99–114.
27. Van Zuylen L, Verweij J, Nooter K, Brouwer E, Stoter G, Sparreboom A. Role of intestinal P-glycoprotein in the plasma and fecal disposition of docetaxel in humans. Clin Cancer Res 2000;6:2598–603.
28. Jain RK. Normalization of tumor vasculature: an emerging concept in antiangiogenic therapy. Science 2005;307:58–62.
29. Kyle AH, Huxham LA, Yeoman DM, Minchinton AI. Limited tissue penetration of taxanes: a mechanism for resistance in solid tumors. Clin Cancer Res 2007;13:2804–10.
30. Shalli K, Brown I, Heys SD, Schofield AC. Alterations of β-tubulin isotypes in breast cancer cells resistant to docetaxel. FASEB J 2005;19:1299–301.
31. Germann UA. P-glycoprotein–a mediator of multidrug resistance in tumour cells. Eur J Cancer 1996;32A:927–44.
32. Badruddoja MA, Krouwer HG, Rand SD, Rebro KJ, Pathak AP, Schmainda KM. Antiangiogenic effects of dexamethasone in 9L gliosarcoma assessed by MRI cerebral blood volume maps. Neuro Oncol 2003;5:235–43.
33. McCune JS, Hawke RL, LeCluyse EL, Gillenwater HH, Hamilton G, Ritchie J, et al. In vivo and in vitro induction of human cytochrome P4503A4 by dexamethasone. Clin Pharmacol Ther 2000;68:356–66.

Downloaded from http://aacrjournals.org/clincancerres/article-pdf/17/14/4814/1997884/4814.pdf by guest on 09 October 2024

34. Kreis W, Budman DR, Calabro A. Unique synergism or antagonism of combinations of chemotherapeutic and hormonal agents in human prostate cancer cell lines. Br J Urol 1997;79:196–202.
35. Wilson C, Scullin P, Worthington J, Seaton A, Maxwell P, O'Rourke D, et al. Dexamethasone potentiates the antiangiogenic activity of docetaxel in castration-resistant prostate cancer. Br J Cancer 2008;99:2054–64.
36. Van der Veldt AA, Luurtsema G, Lubberink M, Lammertsma AA, Hendrikse NH. Individualized treatment planning in oncology: role of PET and radiolabelled anticancer drugs in predicting tumour resistance. Curr Pharm Des 2008;14:2914–31.
37. Dimitrakopoulou-Strauss A, Strauss LG, Schlag P, Hohenberger P, Möhler M, Oberdorfer F, et al. Fluorine-18-fluorouracil to predict therapy response in liver metastases from colorectal carcinoma. J Nucl Med 1998;39:1197–202.
38. Moehler M, Dimitrakopoulou-Strauss A, Gutzler F, Raeth U, Strauss LG, Stremmel W. 18F-labeled fluorouracil positron emission tomography and the prognoses of colorectal carcinoma patients with metastases to the liver treated with 5-fluorouracil. Cancer 1998; 83:245–53.
39. Inoue T, Kim EE, Wallace S, Yang DJ, Wong FC, Bassa P, et al. Positron emission tomography using [18F]fluorotamoxifen to evaluate therapeutic responses in patients with breast cancer: preliminary study. Cancer Biother Radiopharm 1996;11:235–45.

Downloaded from http://aacrjournals.org/clincancerres/article-pdf/17/14/4814/1997884/4814.pdf by guest on 09 October 2024